Journal of Chemical Health Risks

www.jchr.org

JCHR (2024) 14(4), 918-931 | ISSN:2251-6727

Removal of Hazardous Dyes from Aqueous Solutions Using Green-Synthesized Magnetite Nanoparticles via Bauhinia Variegata Leaf Extract: Characterization, Adsorption, Kinetics, and Antimicrobial Studies

Amarapalli Harischandra Prasad[1], Budda Yamuna[2], Putta Sravani[3], Janapareddi Laxmi Mangamma[4], Penmethsa Kiran Kumar[5,] *

[1,2,3,4,5]Department of Chemistry, Government Degree College, Chodavaram, Chodavaram-531036, Andhra Pradesh, India

(Received: 14 April 2024 Revised: 1 May 2024 Accepted: 18 June 2024)

KEYWORDS

Green synthesis, crystal violet, fluorescein sodium, Magnetite nanoparticles.

ABSTRACT:

Green synthesis represents an environmentally friendly and low-cost approach to obtaining Magnetite nanoparticles. In the present study, we synthesized Magnetite nanoparticles (Fe_3O_4-BV NPs) using aqueous leaf extract from Bauhinia variegata. The Fe_3O_4-BV NPs were characterized using UV-visible spectrophotometry, magnetic property, PXRD, FT-IR, SEM, SEM-EDX, TEM, and SAED. As determined from PXRD patterns, the resulting spherical NPs were pure, with a crystallite size of 11.98 nm. VSM studies revealed the superparamagnetic behavior of the NPs. Fe_3O_4-BV NPs were efficient adsorbents for removing crystal violet (CV) and fluorescein sodium (FS) dyes from an aqueous solution. Remarkably, 99% of CV dye was adsorbed in 30 minutes and 95% of FS dye was adsorbed in 90 minutes. Different adsorption models were applied to characterize the dye adsorption process. The maximum equilibrium adsorption capacity of 440.76 mg g^{-1} and 346.32 mg g^{-1} was achieved for CV and FS dyes, respectively. Antimicrobial activity was evaluated using the bacterial strains, gram-positive *Bacillus cereus,* and gram-negative *Escherichia coli*. The study showcased the potential of Fe_3O_4-BV NPs in removing hazardous dyes from aqueous solutions.

1. Introduction

Water pollution due to the contamination of natural waterbodies by dye-containing effluents is one of the greatest challenges faced by mankind. Dyes are widely used in diverse industries such as textiles, paper, leather, and plastics for colouring purposes resulting in a huge quantity of wastewater generation. The release of dye effluents in the untreated form or inadequately untreated form into freshwater bodies has a detrimental effect on aquatic ecosystems and human health. Moreover, the toxic compounds in the dye effluent can accumulate in the environment and bioaccumulate in aquatic organisms thus posing a risk to human health. Hence the removal of dyes is vital and is a challenging task to accomplish for suppressing their ill effects on the human body [1-3].

Different physicochemical methods are employed for removing dyes from wastewater, among which adsorption stands out for its efficiency and cost-effectiveness [4-6]. Numerous materials, including activated carbon, zeolites, MOFs, clays, and biosorbents, have been identified for their exemplary adsorption capabilities [7]. In the realm of adsorbent materials, there is a growing interest in biosorbents derived from renewable and low-cost natural sources, such as agricultural residues, algae, and microorganisms, as eco-friendly alternatives for dye removal from aqueous solution [8-10]. The biosorbents consist of various functional groups, such as carboxyl, amino, hydroxy, and phenoxy, which enable dye adsorption through chemical interactions.

Journal of Chemical Health Risks

www.jchr.org

JCHR (2024) 14(4), 918-931 | ISSN:2251-6727

Green synthesis of nanoparticles is a sustainable, low-cost, and environmentally friendly approach to preparing nanoparticles utilizing natural sources such as plants, microbes, or other biological materials, as reducing and stabilizing agents [11-12]. This approach has several advantages, including low energy consumption, avoidance of hazardous chemicals, and minimal environmental impact. Biological resources such as plant extracts contain compounds like polyphenols, alkaloids, flavonoids, and glycosides which act as reducing and capping agents during nanoparticle synthesis. The properties of the biosynthesized nanoparticles can be tailored by adjusting factors such as temperature, concentration of reactants, and pH. Green synthesized nanoparticles have found applications in diverse fields, including medicine, catalysis, environmental remediation, and electronics [13-15].

Magnetite NPs exhibit distinctive magnetic properties at the nanoscale level. The diminutive size of these particles makes them useful in a broad spectrum of applications [16-20], particularly in environmental remediation for contaminant removal from water and soil [21]. Extracts of different types of plants have been used to prepare the Magnetite NPs by green synthesis [22-23]. However, to date, green synthesis of Magnetite NPs using the leaf extract of Bauhinia variegata has not been reported in the literature. Bauhinia variegata, locally known as Devakanchanamu is found in tropical and subtropical countries [24]. The leaves of Bauhinia variegata are rich in diverse chemical compounds, including carbohydrates, alkaloids, flavonoids, terpenoids, phenolics, tannins, and glucosides, contributing to a range of beneficial activities such as antifungal, anticarcinogenic, antimicrobial, antidiabetic, hypoglycemic activity, haematinic activity, and anti-inflammatory activity [25-26].

In this study, the Magnetite NPs were synthesized using the aqueous leaf extract of Bauhinia variegata. The as-synthesized Magnetite NPs, herein referred to as Fe_3O_4-BV NPs, were well characterized using different analytical techniques. The antimicrobial activity of Fe_3O_4-BV NPs was tested using both the gram-positive *Bacillus cereus* and gram-negative *Escherichia coli* bacterial strains. The Fe_3O_4-BV NPs were employed in adsorption experiments to explore their efficacy in the removal of dyes from the aqueous solution. The adsorption experiments revealed that they were excellent materials for the removal of CV and FS dyes with a removal efficiency of 99% and 95% respectively. The study explored the potential applications of newly green synthesized Fe_3O_4-BV NPs.

2. Materials and Methods

Materials and Instrumentation

Ferric chloride ($FeCl_3$. $6H_2O$), ferrous ammonium sulphate ($(NH_4)_2FeSO_4$. $6H_2O$), crystal violet (CV), and fluorescein sodium (FS), and ammonia were procured from Sigma Aldrich. The Bauhinia variegate leaves were collected from the botanical garden of the Government Degree College, Chodavaram.

The formation of Fe_3O_4-BV NPs was confirmed in the first stage using a magnet and UV-vis spectrophotometer (Shimadzu UV-250). The surface morphology was determined using scanning electron microscopy (JEOL JSM-6390LA). The elemental analysis of synthesized Fe_3O_4-BV NPs was performed via energy-dispersive X-ray spectroscopy (EDS) using an acceleration voltage of 10 kV. The crystalline properties and phase purity of Fe_3O_4-BV NPs were examined by Bruker D8 Advance diffractometer equipped with monochromatized Cu Kα radiation (λ = 1.5406 Å) operated at 40 kV and 40 mA. Different functional groups on the surface of Fe_3O_4-BV NPs were characterized using an FTIR spectrophotometer (Agilent Cary 660) working in the transmission mode in the 400 - 4000 cm^{-1} range. The crystal structure was determined by capturing the TEM images (JEOL JEM-2100. To evaluate the crystallinity of Fe_3O_4-BV NPs, a selected area electron diffraction (SAED) pattern was recorded. The magnetic properties were studied at 300 K using a vibrating sample magnetometer (VSM, Lakeshore VSM 7410) with a field sweeping from −15,000 to + 15,000 Oe.

Preparation of Bauhinia variegata leaf extract

1 g of *Bauhinia variegata* leaf powder was added to a round-bottom flask containing 100 mL of distilled water. The solution is boiled at 60 ℃ with stirring at rpm of 300 for 60 minutes. After boiling, The extract was cooled to room temperature and filtered using Whatman filter paper. The leaf extract was kept at 4 ℃ until further use.

Green Synthesis of Fe_3O_4-BV NPs

Fe_3O_4-BV NPs were synthesized following the procedure described by Yew et al with some modifications [27].

Journal of Chemical Health Risks

www.jchr.org

JCHR (2024) 14(4), 918-931 | ISSN:2251-6727

0.80 g (2 millimoles) of ferrous ammonium sulphate ($(NH_4)_2FeSO_4$. $6H_2O$) was dissolved in 100 mL of distilled water and sonicated for 10 minutes. 1.0 g (4.2 millimoles) of ferric chloride ($FeCl_3$. $6H_2O$) was added to the solution and sonicated for 10 minutes. The resultant solution was heated at 80 ℃ with stirring at 300 rpm for 30 minutes. Subsequently, 10 mL of leaf extract was added and the mixture was heated at 80 ℃ with stirring at rpm of 300 for 10 minutes. Following this, 1 M ammonia solution was added dropwise with stirring at 300 rpm until the pH of the solution mixture reached 11. The black-colored precipitate of Fe_3O_4-BV NPs was obtained. After cooling to room temperature, a magnet separated the precipitate from the solution. The obtained Fe_3O_4-BV NPs were washed several times with distilled water and then dried in the oven at 80 ℃ overnight.

Adsorption experiments

Adsorption batch experiments were conducted to determine the optimum conditions for adsorption of crystal violet (CV) and fluorescein sodium (FS) dyes by variable amounts of Fe_3O_4-BV NPs (10-50 mg), varying the pH (3-11) of the dye solutions, contact time (5-90 minutes) of Fe_3O_4-BV NPs with dye solutions, and using 100 mL of CV and FS dye solutions with different initial concentrations (10-50 mg L^{-1}). CV and FS dye stock solutions were prepared by dissolving 1000 mg of the dye in 1000 mL of distilled water. CV and FS Dye solutions with desired concentrations were prepared by diluting these solutions. The adsorption capacity at equilibrium (q_e) was calculated using the equation .

$$q_e = \frac{V(C_o - C_e)}{M}$$

Where C_o is the initial dye concentration (mg L^{-1}), C_e is the dye concentration (mg L^{-1}) at equilibrium, V is the volume of the dye solution (L) and M is the mass of Fe_3O_4-BV NPs. Ten milligrams of Fe_3O_4-BV NPs were added to each of the 100 mL dye solutions having a concentration of 10, 20, 30, 40, and 50 mg L^{-1}. After 30 minutes for CV dye and 90 minutes for FS dye, the absorbance of each solution was measured and the C_e values were determined from the absorbance values using the calibration curve.

The percentage removal of dye was calculated using the equation. .

$$\text{percentage removal} = \frac{(C_o - C_e)}{C_o} \times 100$$

Adsorption isotherms were studied using different adsorption isotherm models, Freundlich, Langmuir, and Temkin [28].

Freundlich adsorption isotherm is expressed as the equation.

$$ln\, q_e = ln\, K_F + \frac{1}{n} ln\, C_e$$

Where K_F is the Freundlich constant, and n is the constant.

Langmuir adsorption isotherm is represented by the equation.

$$\frac{C_e}{q_e} = \frac{C_e}{q_m} + \frac{1}{q_m K_L}$$

Where q_m is the maximum adsorption capacity (mg g^{-1}) of the adsorbent (Fe_3O_4-BV NPs) with the highest concentration of dye (50 mg L^{-1}) used in the adsorption experiment, and K_L is the Langmuir adsorption constant.

Temkin adsorption isotherm is given by the equation.

$$q_e = \frac{RT}{B_T} ln\, C_e + \frac{RT}{B_T} ln\, K_T$$

Where B_T is the adsorption heat constant (J) and K_T is the equilibrium binding constant (L mg^{-1}).

Adsorption kinetics

For the kinetic study, 100 mL of dye solution having a concentration of 10 mg L^{-1} and 10 mg of Fe_3O_4-BV NPs as adsorbent was used. At the desired time (t), the dye solutions were withdrawn and the absorbance was measured. The dye amounts adsorbed at a time 't', q_t (mg g^{-1}) were calculated using the equation.

$$q_t = \frac{V\,(C_o - C_t)}{M}$$

Where C_t is the dye concentration (mg L^{-1}) at time t (min).

Kinetic models, pseudo-first-order (PFO), pseudo-second-order (PSO), and Intraparticle diffusion (IPD) were applied to study the rate of removal of CV and FS dyes by adsorption [29].

Pseudo-first-order (PFO) kinetics,

$$ln(q_e - q_t) = ln\, q_e - k_1 t$$

Journal of Chemical Health Risks

www.jchr.org

JCHR (2024) 14(4), 918-931 | ISSN:2251-6727

Pseudo-second-order (PSO) kinetics,

$$\frac{t}{q_t} = \frac{1}{k_2 q_e^2} + \frac{1}{q_e} t$$

Intraparticle diffusion (IPD) kinetics,

$$q_t = k_i t^{1/2} + C$$

Where k_1 (min^{-1}), k_2 (g mg^{-1} min^{-1}), and k_i (mg g^{-1} $min^{-1/2}$) are the rate constants for PFO, PSO, and IPD kinetics respectively. C is the intraparticle diffusion constant.

Antimicrobial studies

The antimicrobial activity of Bauhinia variegata leaf extract and Fe_3O_4-BV NPs was evaluated against two bacterial strains, gram-positive *Bacillus cereus*, and gram-negative *Escherichia coli* by employing the agar well diffusion method. For the antimicrobial study, Fe_3O_4-BV NPs and leaf extract with a concentration of 1 µg mL^{-1}, 2 µg mL^{-1}, and 5 µg mL^{-1} were used. Ciprofloxacin, at a concentration of 5 µg mL^{-1}, served as the positive control. Each experiment was repeated three times for each bacterial strain.

Results and discussion

Formation of Fe_3O_4-BV NPs

The formation of Fe_3O_4-BV NPs was confirmed by the noticeable colour change of the reaction mixture from light brown to black during the synthesis, coupled with their magnetic properties. The NPs were separated from the reaction mixture using a magnet. Previous studies suggest that phytochemicals, such as polyphenols or flavonoids present in the aqueous *Bauhinia variegata* leaf extract, may play crucial roles in both the formation and capping of the nanoparticles [22, 30].

Characterization of Fe_3O_4-BV NPs

The synthesized Fe_3O_4-BV NPs were characterized using various analytical techniques. The UV-visible spectra of *Bauhinia variegata* leaf extract and Fe_3O_4-BV NPs are shown in Figure 1. In the spectrum of Fe_3O_4-BV NPs, no characteristic peak was observed in the UV-visible region. The broad spectrum formed may be attributed to the reaction between the phytochemicals of leaf extract and iron salts. It closely resembled the typical UV-visible spectrum of iron-based NPs reported in the literature [22].

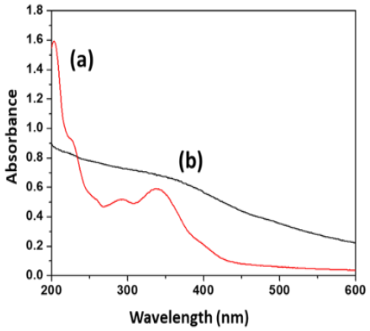

Figure 1. UV-visible spectrum of (a) *Bauhinia variegata* leaf extract and (b) Fe_3O_4-BV NPs

In Figure 2, the FTIR spectra of Bauhinia variegata leaf extract and Fe_3O_4-BV NPs are presented. In the FTIR spectrum of the *Bauhinia variegata* leaf extract, the bands observed at 3306 cm^{-1} and 1632 cm^{-1} were attributed to the presence of the O-H group of phenolic compounds and the carbonyl group of carboxylic acid, respectively. In the FTIR spectrum of Fe_3O_4-BV NPs, a band around 3200 cm^{-1} was assigned to the stretching frequency of the phenolic O-H group, likely originating from the leaf extract. The band at 1620 cm^{-1}, was ascribed to the carbonyl group of carboxylic acid, which acts as a capping agent. A band at 1118 cm^{-1} was assigned to the stretching frequency of the phenolic C-O group. A strong absorption band observed at 534 cm^{-1} indicates the presence of Fe-O bonds in the synthesized Fe_3O_4-BV NPs.

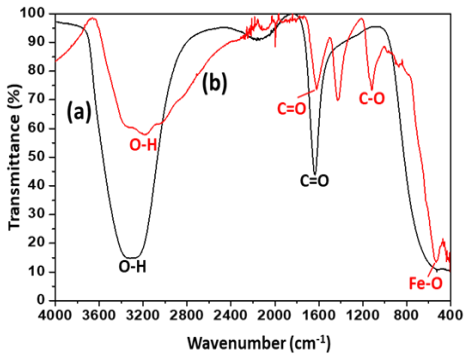

Figure 2. FT-IR spectrum of (a) *Bauhinia variegata* leaf extract and (b) Fe_3O_4-BV NPs

In Figure 3a, the PXRD patterns of the Fe_3O_4-BV NPs are displayed. Consistent with earlier studies, five characteristic diffraction peaks at 2θ values of 30.42°, 35.81°, 43.49°, 57.48°, and 63.08° were observed, corresponding to the (220), (311), (400), (511), and (440) planes, respectively. These observed diffraction peaks

Journal of Chemical Health Risks

www.jchr.org

JCHR (2024) 14(4), 918-931 | ISSN:2251-6727

were matched well with the standard PXRD patterns of Fe_3O_4 with inverse spine structure (JCPDS Card No. 19-0629), confirming the crystallinity of the synthesized Fe_3O_4-BV NPs. The intense peak at 35.81° indicates the abundance of (311) planes in Fe_3O_4-BV NPs. The crystallite size of Fe_3O_4-BV NPs was calculated using the Scherrer Equation.

$$D = \frac{k\lambda}{\beta_{311} Cos\theta_{311}}$$

Where D is the average crystallite size, k is a constant and is equal to 0.9, λ is the wavelength of X-rays (0.154 nm), β_{311} is the width (full-width at half-maximum) of the X-ray diffraction peak (in radians), and θ_{311} is the Bragg angle corresponding to (311) plane. The mean crystallite size of Fe_3O_4-BV NPs was determined to be 11.98 nm.

Figure 3b shows the SEM image of Fe_3O_4-BV NPs. The nanoparticles were observed to have a spherical shape, with aggregations of particles. These aggregations may stem from interactions between Fe_3O_4-BV NPs and phytochemicals, alongside the inherent magnetic properties of the nanoparticles [31].

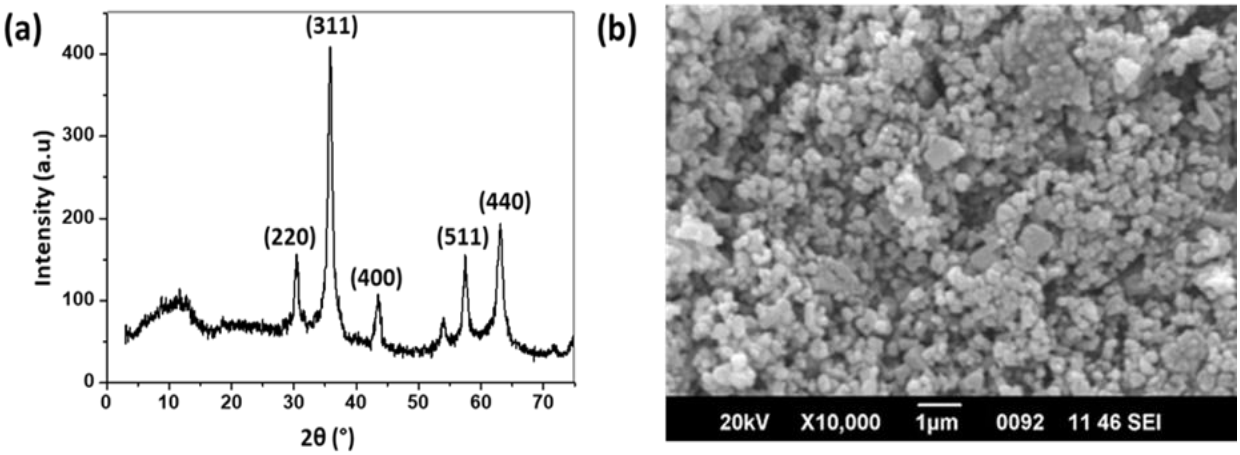

Figure 3. (a) PXRD patterns and (b) SEM image of Fe_3O_4-BV NPs

The EDS spectrum of Fe_3O_4-BV NPs is presented in Figure 4a. Intense peaks at 6.398 keV (Kα line) and 0.525 keV (Kα line) confirmed the presence of iron and oxygen respectively in Fe_3O_4-BV NPs. A peak at 0.705, corresponding to the Lα line of iron, is also present in the spectrum. Such spectra are consistent with findings reported in numerous studies [32]. The TEM image of Fe_3O_4-BV NPs in Figure 4b shows that the particles have a spherical structure. Using ImageJ, the average size of 50 particles in the TEM image was determined. The diameter of particles was plotted as a histogram and fitted with Gaussian distribution, as illustrated in Figure 4c. The average diameter of Fe_3O_4-BV NPs was 12.53 nm, closely matching the PXRD result of 11.98 nm.

The selected area electron diffraction (SAED) pattern of Fe_3O_4-BV NPs is shown in Figure 4d. The SAED pattern reveals concentric rings with intermittent dots, characteristic of polycrystalline NPs. The magnetization curve obtained from VSM is presented in Figure 4e. From the curve, it is evident that the synthesized NPs are displaying superparamagnetic behavior in the presence of an external magnetic field [30]. The superparamagnetism of NPs can be attributed to their small size enabling them to behave as single-domain particles [33].

Journal of Chemical Health Risks

www.jchr.org

JCHR (2024) 14(4), 918-931 | ISSN:2251-6727

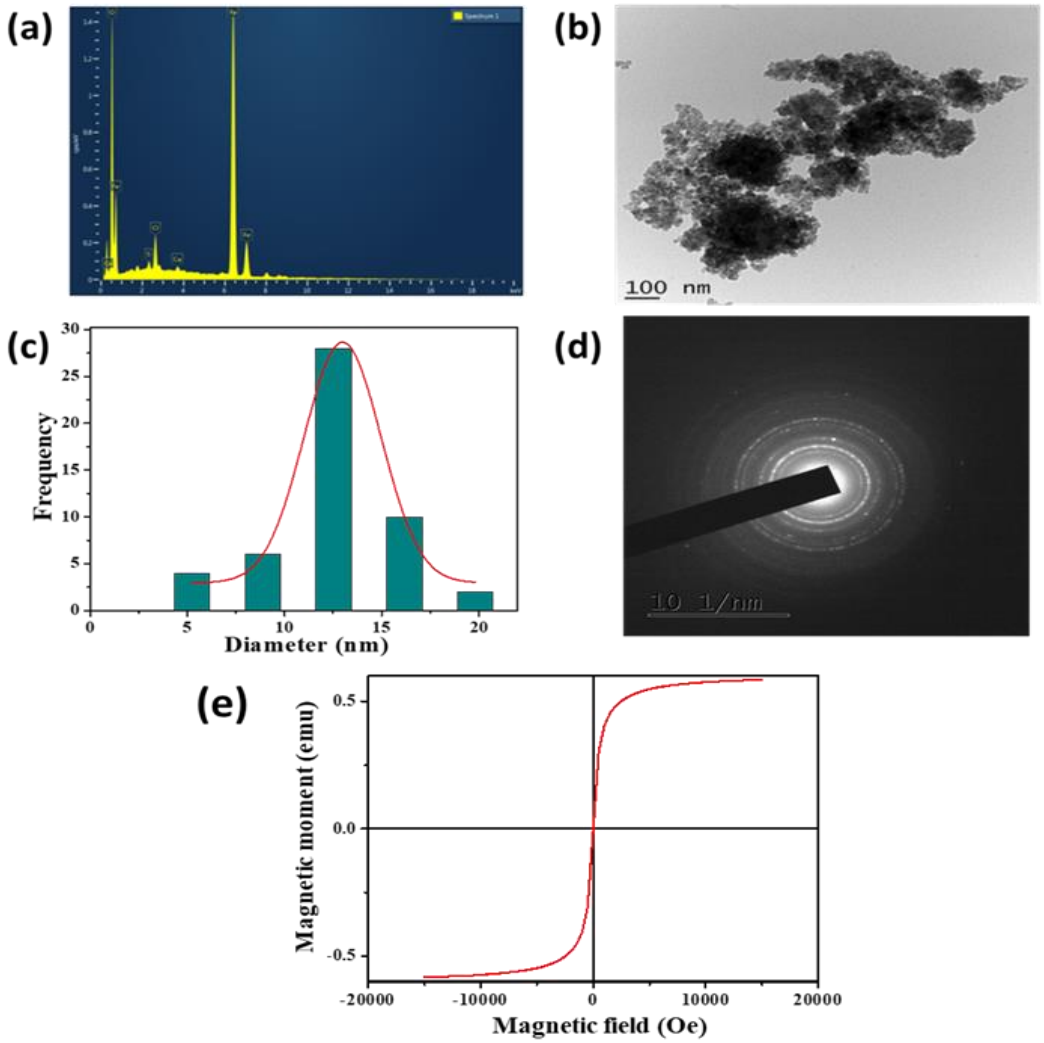

Figure 4. (a) EDS spectrum of Fe_3O_4-BV NPs. (b) TEM image of Fe_3O_4-BV NPs. (c) Particle size distribution of Fe_3O_4-BV NPs from TEM image. (d) SAED patterns of Fe_3O_4-BV NPs (e) Magnetization curve of Fe_3O_4-BV NPs

Effect of initial CV and FS dye concentration

To investigate the influence of initial dye concentration on adsorptive removal, separate experiments were conducted using 10 mg of Fe_3O_4-BV NPs with varying initial concentrations of CV and FS dyes ranging from 10 to 50 mg L^{-1}. The results are presented in Figure 5a. The equilibrium time for adsorption was 30 minutes for CVdye and 90 minutes for FS dye As the initial dye concentration increased from 10 to 50 mg L^{-1}, the CV dye removal percentage decreased from 99.9% to 88.0%, and the FS dye removal percentage decreased from 95.3% to 80.2%.

Effect of Fe_3O_4-BV NPs dose

The impact of varying doses of Fe_3O_4-BV NPs on the percentage removal of CV and FS dyes from aqueous solution was illustrated in Figure 5b. Doses ranging from 2 to 10 mg of Fe_3O_4-BV NPs were added to each 100 mL of 10 mg L^{-1} CV and FS dye aqueous solutions. The percentage removal of both the CV and FS dyes increased with an increase in Fe_3O_4-BV NP's dose from 2 mg to 10 mg. This trend can be attributed to the increase in the surface area of the adsorbent, Fe_3O_4-BV NPs. With a 10 mg dose of Fe_3O_4-BV NPs, maximum removal percentages of 99.89 and 95.26 were achieved for CV and FS dyes respectively.

Journal of Chemical Health Risks

www.jchr.org

JCHR (2024) 14(4), 918-931 | ISSN:2251-6727

Effect of contact time

The effect of contact time between dye solutions and Fe_3O_4-BV NPs on the removal percentage of CV and FS dyes was studied, and the results are presented in Figure 5c and Figure 5d, respectively. A decrease in CV dye removal percentage was noted after 20 minutes, reaching equilibrium at 30 minutes. Similarly, FS dye adsorption followed a comparable trend, with equilibrium achieved at 90 minutes.

Effect of pH

The study of the effect of the pH of the solution is of great importance as it significantly influences the adsorptive removal of dyes. pH impacts both the surface charge of the adsorbent and the ionization of dye molecules. Adsorption experiments were conducted using single CV and FS dye aqueous solutions, each with an initial concentration of 10 mg L^{-1}, employing 10 mg of Fe_3O_4-BV NPs adsorbent for 30 minutes and 90 minutes, respectively. Maximum adsorption of cationic CV dye and anionic FS dye was observed at a pH of 10 and 5.5, respectively. These results align with the Fe_3O_4-BV NPs pHzpc value of 7.4. At pH levels above this value, the adsorbent carries a negative charge, favoring the adsorption of CV dye in its cationic form through electrostatic interactions. Conversely, at pH lower than 7.4, the adsorbent carries a positive charge, facilitating the adsorption of FS dye in its anionic form through electrostatic interactions.

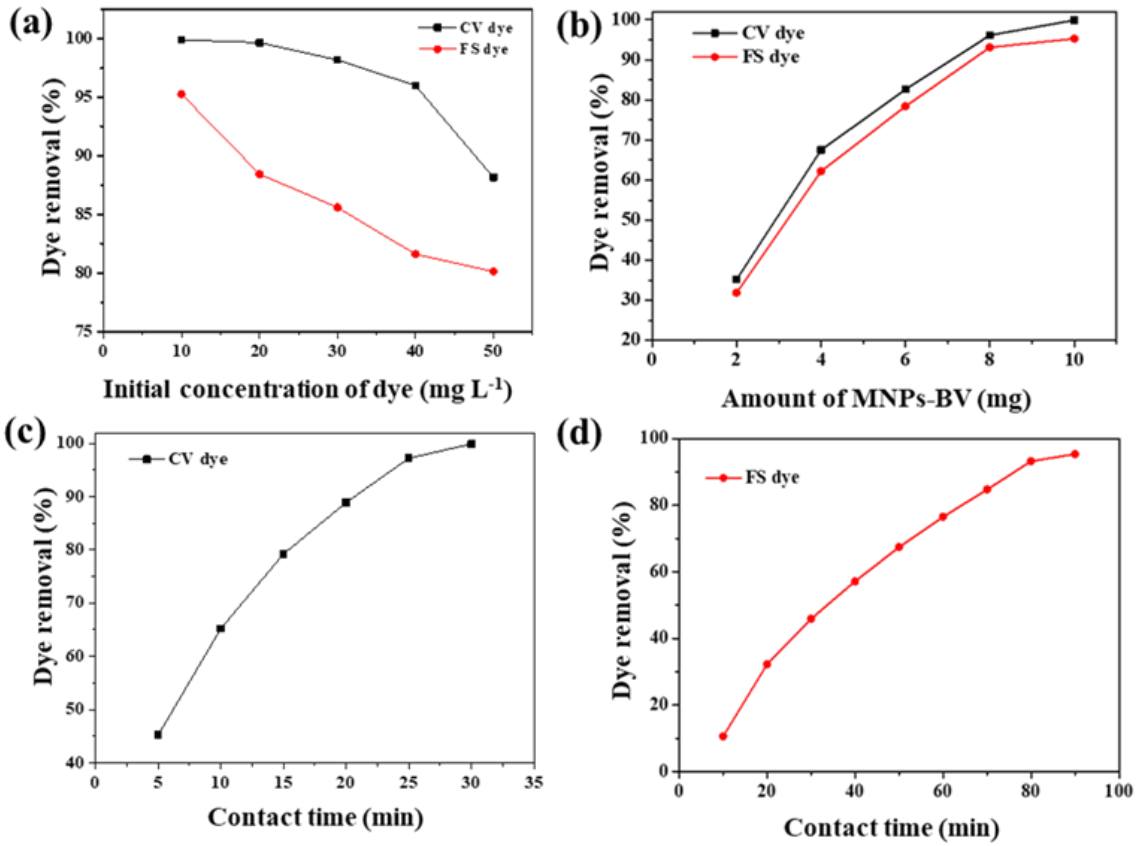

Figure 5. Factors affecting the adsorption of CV and FS dyes onto Fe_3O_4-BV NPs (a) Initial concentration of dye. (b) Amount of Fe_3O_4-BV NPs. (c) Contact time for CV dye adsorption. (d) Contact time for FS dye adsorption.

Journal of Chemical Health Risks

www.jchr.org

JCHR (2024) 14(4), 918-931 | ISSN:2251-6727

Adsorption isotherms

Three distinct adsorption isotherm models, Freundlich, Langmuir, and Temkin, were applied to determine the adsorption capacity of synthesized Fe_3O_4-BV NPs. The best fit for the adsorption data was found using the linear form of the three adsorption models. The linear plots for Freundlich, Langmuir, and Temkin isotherms for CV dye and FS dye adsorption are depicted in Figures 6-8. Based on Coefficient of determination (R^2) values, the Langmuir model (R^2 = 0.9961 for CV dye and 0.9986 for FS dye) was the best fit compared to the Freundlich model (R^2 = 0.9664 for CV dye and 0.9481 for FS dye) and Temkin model (R^2 = 0.9680 for CV dye and 0.9887 for FS dye).

The adsorption isotherm parameters for the three models are listed in Table 1. From the slope of the plot in Figure 7a, the calculated maximum adsorption capacity ($q_{m,\,cal}$) of the Fe_3O_4-BV NPs for CV dye was found to be 452.49 mg g^{-1}, which closely matched the experimental maximum adsorption capacity ($q_{m,\,exp}$) value of 440.76 mg g^{-1}. Similarly, from the slope of the plot in Figure 7b, the calculated maximum adsorption capacity ($q_{m,\,cal}$) of the Fe_3O_4-BV NPs for FS dye was found to be 395.32 mg g^{-1}, which was close to the experimental maximum adsorption capacity ($q_{m,\,exp}$) value of 346.32 mg g^{-1}.

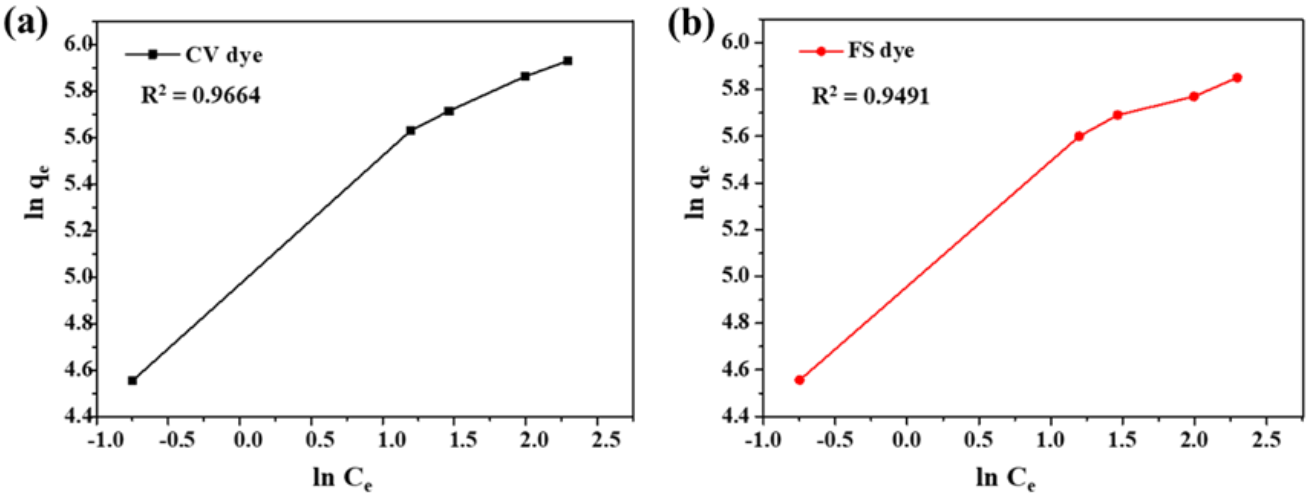

Figure 6. Linear plot of Freundlich isotherm for (a) CV dye and (b) FS dye

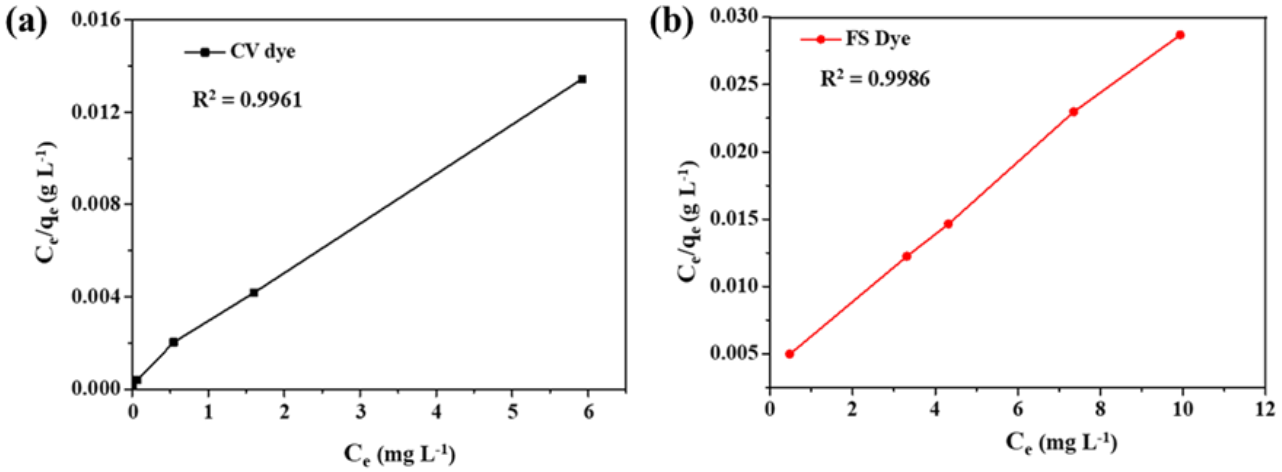

Figure 7. Linear plot of Langmuir isotherm for (a) CV dye and (b) FS dye

Journal of Chemical Health Risks
www.jchr.org
JCHR (2024) 14(4), 918-931 | ISSN:2251-6727

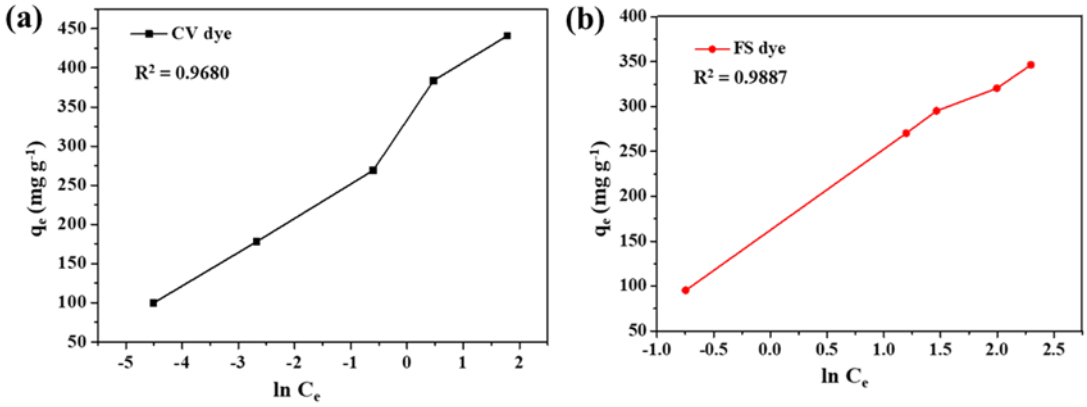

Figure 8. Linear plot of Temkin isotherm for (a) CV dye and (b) FS dye

Table 1. Isotherm parameters for adsorption of CV and FS dyes on Fe_3O_4-BV NPs

Dye	$q_{e,exp}$ (mg g^{-1})	Freundlich isotherm			Langmuir isotherm			Temkin isotherm		
		n	K_F (mg g^{-1})	R^2	q_m (mg g^{-1})	K_L (L mg^{-1})	R^2	B_T (J $mole^{-1}$)	K_T (L g^{-1})	R^2
CV	440.76	2.15	142.72	0.9664	452.49	5.26	0.9961	44.6	423	0.9680
FS	346.32	2.296	141.17	0.9491	395.26	0.6588	0.9986	29.9	7.09	0.9887

The adsorption capacity of Fe_3O_4-BV NPs for the adsorption of CV and FS dyes was compared with various other adsorbents reported in the literature as shown in Table 2.

Table 2. Comparison with other adsorbents for adsorption of CV and FS dyes

Dye	Adsorbent	Adsorption capacity (mg g^{-1})	Reference
CV	Fe_3O_4-BV NPs	440.76	Present work
	Zr-NDC MOF	452.2	[34]
	ACL	23.6	[35]
	MS	259.2	[36]
	CHP	454.2	[37]
	PH	20.95	[38]

Journal of Chemical Health Risks

www.jchr.org

JCHR (2024) 14(4), 918-931 | ISSN:2251-6727

	Trifolium repens	1.952	[39]
	AC fabrics	428	[40]
FS	Fe_3O_4-BV NPs	346.32	Present work
	MOF-808	480.2	[41]
	NPS	0.4	[42]

Kinetics studies

The data obtained from kinetic studies was used to determine the optimal kinetic model for the adsorption of CV and FS dyes by Fe_3O_4-BV NPs. The linear plots for the three distinct models are depicted in Figures 9-11. The kinetic parameters are listed in Table 3. Based on Coefficient of determination (R^2) values, the pseudo-second-order (PSO) model emerged as the best fit for the adsorption of both CV and FS dyes. These findings suggest that the adsorption of both dyes onto the surface of Fe_3O_4-BV NPs is primarily due to chemisorption.

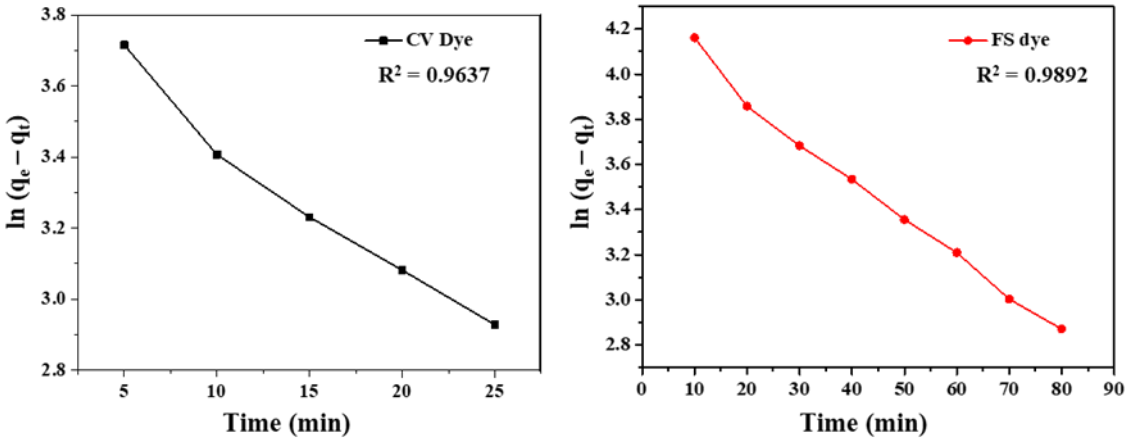

Figure 9. Linear plot of Pseudo-first-order (PFO) kinetics of adsorption for (a) CV dye and (b) FS dye

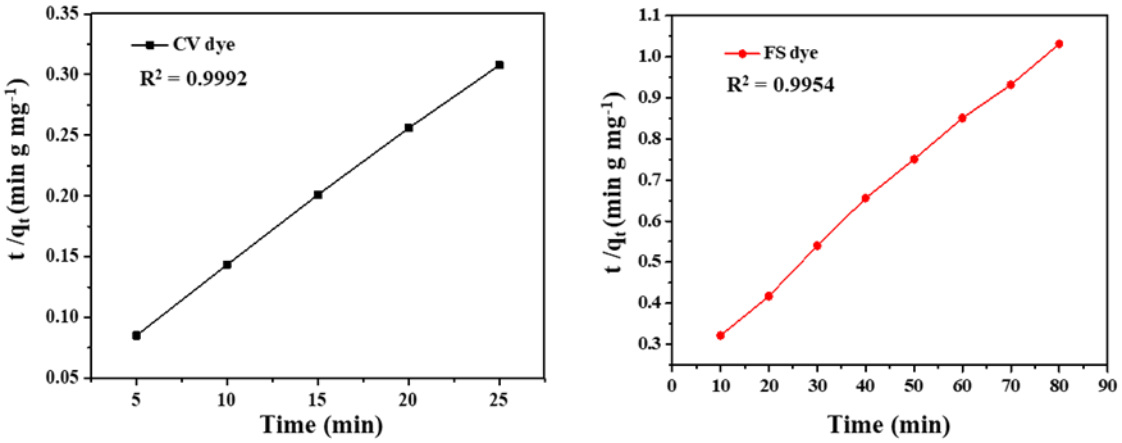

Figure 10. Linear plot of Pseudo-second-order (PSO) kinetics of adsorption for (a) CV dye and (b) FS dye

Journal of Chemical Health Risks

www.jchr.org

JCHR (2024) 14(4), 918-931 | ISSN:2251-6727

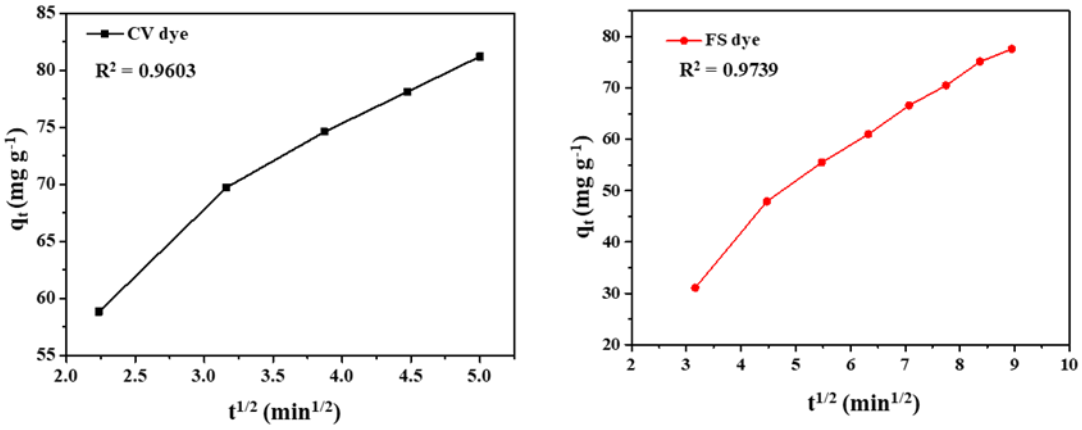

Figure 11. Linear plot of Intraparticle diffusion (IPD) kinetics of adsorption for (a) CV dye and (b) FS dye

Table 3. Kinetic parameters for adsorption of CV and FS dyes on Fe_3O_4-BV NPs

Dye	Pseudo-first-order model			Pseudo-second-order model			Intraparticle diffusion model		
	$q_{e,cal}$ (mg g^{-1})	k_1 (min^{-1})	R^2	$q_{e,cal}$ (mg g^{-1})	k_2 (g $mg^{-1}min^{-1}$)	R^2	k_i (mg $g^{-1}min^{-1/2}$)	C	R^2
CV	46.04	0.038	0.9637	85.47	0.00439	0.9992	7.93	42.78	0.9603
FS	70.63	0.018	0.9892	99.10	0.00044	0.9954	7.73	10.82	0.9739

Antimicrobial activity

Antimicrobial studies showed that Bauhinia variegata leaf extract exhibits no antimicrobial activity against two bacterial strains, namely gram-positive *Bacillus cereus* and gram-negative *Escherichia coli*. The mean and standard deviation of the zone of inhibition values were computed and presented in Table 4. The minimum inhibitory concentration (MIC) value of Fe_3O_4-BV NPs for both bacterial strains was 5 µg/mL, as shown in Figure 12. The study indicates that the Fe_3O_4-BV NPs exhibit small to medium antimicrobial activity against bacterial strains.

Table 4. The mean and standard deviation of the zone of inhibition values for bacterial strains and standard

Bacterial strain	Concentration of Fe_3O_4-BV NPs			Concentration of Ciprofloxacin (standard)
	5 µg mL^{-1}	10 µg mL^{-1}	15 µg mL^{-1}	5 µg mL^{-1}
Bacillus cereus	10 ± 0	10.33 ± 0.47	11.33 ± 0.47	27 ± 0.82
Escherichia coli	10.33 ± 0.47	10.66 ± 0.47	13 ± 0.82	29 ± 0.82

Journal of Chemical Health Risks

www.jchr.org

JCHR (2024) 14(4), 918-931 | ISSN:2251-6727

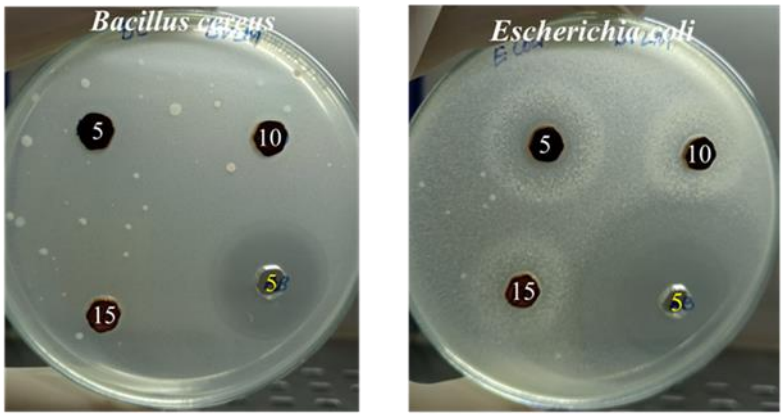

Figure 12. Antimicrobial activity of synthesized Fe_3O_4-BV NPs against (a) *Bacillus cereus* and (b) *Escherichia coli*

Conclusions

A green and sustainable synthesis method was used for preparing Magnetite nanoparticles (Fe_3O_4-BV NPs) using the aqueous leaf extract of *Bauhinia variegata*. The as-synthesized Fe_3O_4-BV NPs exhibited superparamagnetism and were found to be promising adsorbents for the removal of CV and FS dyes from aqueous solutions, with an adsorption maximum of 440.76 mg g^{-1} and 346.32 mg g^{-1} for CV and FS dyes, respectively. Adsorption studies revealed that the Langmuir model is the best fit for the adsorption of both CV and FS dyes from individual dye aqueous solutions. The pseudo-second-order model was the most suitable model to describe the kinetics of CV and FS dye adsorption. The antimicrobial activity of Fe_3O_4-BV NPs was also explored using the gram-positive *Bacillus cereus* and gram-negative *Escherichia coli*. The study highlighted the potential application of green synthesized Fe3O4-BV NPs for adsorptive removal of dyes from aqueous solution.

Conflicts of interest

The authors declare that they have no conflicts of interest.

References

1. Raina, S., Roy, A., Bharadvaja, N., 2020. Degradation of dyes using biologically synthesized silver and copper nanoparticles. Environmental Nanotechnology, Monitoring & Management 13, 100278.
2. Sharma, J., Sharma, S., Soni, V., 2021. Classification and impact of synthetic textile dyes on Aquatic Flora: A review. Regional Studies in Marine Science. 45, 101802.
3. Al-Tohamy, R., Ali, S.S., Li, F., Okasha, K.M., Mahmoud, Y.A., et al. 2022. A critical review on the treatment of dye-containing wastewater: Ecotoxicological and health concerns of textile dyes and possible remediation approaches for environmental safety. Ecotoxicology and Environmental Safety. 231, 113160.
4. Dutta, S., Gupta, B., Srivastava, S.K., Gupta, A.K., 2021. Recent advances on the removal of dyes from wastewater using various adsorbents: a critical review. Materials Advances. 14(2), 4497- 4531.
5. Katheresan, V., Kansedo, J., Lau, S.Y., 2018. Efficiency of Various Recent Wastewater Dye Removal Methods: A Review. Journal of Environmental Chemical Engineering. 6 (4), 4676-4697.
6. Mamun, K.R., Saha, N.K., Chakrabarty, S., 2019. A Comparative study of the adsorption capacity of Tea leaves and orange peel for the removal of Fe(III) Ion from wastewater. Journal of Chemical Health Risks. 9(2), 107-115.
7. Zhou, Y., Lu, J., Zhou, Yi., Liu, Y., 2019. Recent advances for dyes removal using novel adsorbents: A review. Environmental Pollution. 252 (Part A): 352-365.
8. Aragaw, T.A., Bogale, F.M., 2021. Biomass-based adsorbents for removal of dyes from wastewater: a

review. Frontiers in Environmental Science, 9, 764958.

9. Elgarahy, A.M., Elwakeel K.Z., Mohammad, S.H., Elshoubaky, G.A., 2021. A critical review of biosorption of dyes, heavy metals and metalloids from wastewater as an efficient and green process. Cleaner Engineering and Technology. 4, 100209.
10. Caicedo, O., Devia-Ramirez, J., Malagón, A., 2018. Adsorption of Common Laboratory Dyes Using Natural Fibers from Luffa cylindrica. Journal of Chemical Education. 95 (12), 2233-2237.
11. Ying, S., Guan, Z., Ofoegbu, P. C., Clubb, P., Rico, C., He, F., Hong, J., 2022. J. Green synthesis of nanoparticles: Current developments and limitations. Environmental Technology & Innovation. 26, 102336.
12. Verma, R., Pathak, S., Srivastava, A.K., Prawer, S., Tomljenovic-Hanic, S., 2021. ZnO nanomaterials: Green synthesis, toxicity evaluation and new insights in biomedical applications. Journal of Alloys and Compounds. 876, 160175.
13. Bordiwala, R.V., 2023. Green synthesis and applications of metal nanoparticles.-A review article. Results in Chemistry. 5, 100832.
14. Vijayaram, S., Razafindralambo, H., Sun, Y.Z., Vasantharaj, S., Ghafarifarsani, H., Hoseinifar, S.H., Raeeszadeh, M., 2024. Applications of green synthesized metal nanoparticles-a review. Biological Trace Element Research. 202(1), 360-86.
15. Tejaswini, G., Lakshmi Kishore, P., Kiran Kumar, P., Lakshmi Rekha, B., Bhagya Lakshmi, K., 2023. Biodesigned ZnO nanoparticles with leaves of elaeocarpus sylvestris and investigation of photocatalyst for dye degradation and antimicrobial applications. Arabian Journal for Science and Engineering. 49 (1), 181-93.
16. Gul, S., Khan, S.B., Rehman, I.U., Khan, M.A., Khan, M.I., 2019. A comprehensive review of magnetic nanomaterials modern day theranostics. Frontiers in Materials. 6, 179.
17. Zhang, Q., Yang, X., Guan, J., 2019. Applications of magnetic nanomaterials in heterogeneous catalysis. ACS Applied Nano Materials. 2(8), 4681-97.
18. Liu, M., Ye, Y., Ye, J., Gao, T., Wang, D., Chen, G., Song, Z., 2023. Recent advances of magnetite (Fe_3O_4)-based magnetic materials in catalytic applications. Magnetochemistry. 9(4), 110.
19. Yang, C., Wu, J., Hou, Y., 2011. Fe_3O_4 nanostructures: synthesis, growth mechanism, properties and applications. Chemical Communications. 47(18), 5130-41.
20. Shen, Y., Jiang, B., Xing, Y., 2021. Recent advances in the application of magnetic Fe_3O_4 nanomaterials for the removal of emerging contaminants. Environmental Science and Pollution Research. 28(7), 7599-7620.
21. Dhar, P.K., Saha, P., Hasan, M.K., Amin, M.K., Haque, M.R., 2021. Green synthesis of magnetite nanoparticles using Lathyrus sativus peel extract and evaluation of their catalytic activity. Cleaner Engineering and Technology. 3, 100117.
22. Nguyen, M.D., Tran, H.V., Xu, S., Lee, T.R., 2021. Fe_3O_4 nanoparticles: structures, synthesis, magnetic properties, surface functionalization, and emerging applications. Applied Sciences. 11(23), 11301.
23. Sharma, K., Kumar, V., Kumar, S., Sharma, R., Mehta, C.M., 2021. Bauhinia variegata: a comprehensive review on bioactive compounds, health benefits and utilization. Advances in Traditional Medicine. 21, 645-653.
24. Abdel-Halim, A.H., Fyiad, A.A., Aboulthana, W.M., El-Sammad, N.M., Youssef, A.M., Ali, M.M., 2020. Assessment of the anti-diabetic effect of Bauhinia variegata gold nano-extract against streptozotocin induced diabetes mellitus in rats. Journal of Applied Pharmaceutical Science. 10(05), 077-91.
25. Mishra, A., Sharma, A.K., Kumar, S., Saxena, A.K., Pandey, A.K., 2013. Bauhinia variegata leaf extracts exhibit considerable antibacterial, antioxidant, and anticancer activities. BioMed Research International. 2013, 915436.
26. Yew, Y.P., Shameli, K., Miyake, M., Kuwano, N., Ahmad Khairudin et al., 2016. Green magnetite (Fe_3O_4) nanoparticle synthesis using seaweed (Kappaphycus alvarezii) extract. Nanoscale research letters. 11, 1-7.
27. Ragadhita, R., Nandiyanto, A.B., 2021. How to calculate adsorption isotherms of particles using two-parameter monolayer adsorption models and equations. Indonesian Journal of Science and Technology. 6(1), 205-34.
28. Kiran Kumar, P., Satya Veni, S., 2023. Ultrasound-Assisted Synthesis of Defective MOF-801 for the Adsorptive Removal of Cationic Dyes. Iranian

Journal of Chemical Health Risks

www.jchr.org

JCHR (2024) 14(4), 918-931 | ISSN:2251-6727

Journal of Chemistry and Chemical Engineering. 42 (10), 3293-3305.

29. Ghoohestani, E., Samari, F., Homaei, A., Yosuefinejad, S.A., 2024. Facile strategy for preparation of Fe_3O_4 magnetic nanoparticles using Cordia myxa leaf extract and investigating its adsorption activity in dye removal. Scientific Reports. 14(1), 84.
30. de Jesús Ruíz-Baltazar, Á., Reyes-López, S.Y., de Lourdes Mondragón-Sánchez, M., Robles-Cortés, A.I., Pérez, R., 2019. Eco-friendly synthesis of Fe_3O_4 nanoparticles: evaluation of their catalytic activity in methylene blue degradation by kinetic adsorption models. Results in Physics.12, 989-95.
31. Nawaz, T., Zulfiqar, S., Sarwar, M.I., Iqbal, M., 2020. Synthesis of diglycolic acid functionalized core-shell silica coated Fe_3O_4 nanomaterials for magnetic extraction of Pb (II) and Cr (VI) ions. Scientific Reports. 10(1), 10076.
32. Sezer, N., Arı, İ., Bicer, Y., Koc, M., 2021. Superparamagnetic nanoarchitectures:Multimodal functionalities and applications. Journal of Magnetism and Magnetic Materials. 538, 168300.
33. Kiran Kumar, P., Satya Veni, S., 2022. Adsorptive removal of crystal violet from aqueoussolution by ultrasonic-assisted synthesized zirconium-2,6-naphthalenedicarboxylate metal-organic framework. Turkish Journal of Chemistry, 46 (6), 1972-83.
35. Foroutan, R., Peighambardoust, S.J., Peighambardoust, S.H., Pateiro, M., Lorenzo, J.M., 2021. Adsorption of crystal violet dye using activated carbon of lemon wood and activated carbon/Fe_3O_4 magnetic nanocomposite from aqueous solutions: a kinetic, equilibrium and thermodynamic study. Molecules. 26(8), 2241.
36. Li, Y., Wang, S., Shen, Z., Li, X., Zhou, Q., 2020. Gradient adsorption of methylene blue and crystal violet onto compound microporous silica from aqueous medium. ACS omega. 5(43), 28382-92.
37. Sultana, S., Islam, K., Hasan, M.A., Khan, H.J., Khan, M.A., 2022. Adsorption of crystal violet dye by coconut husk powder: isotherm, kinetics and thermodynamics perspectives. Environmental Nanotechnology, Monitoring & Management. 17, 100651.
38. Abbas, S., Javeed, T., Zafar, S., Taj, M.B., Ashraf, A.R., 2021. Adsorption of crystal violet dye by using a low-cost adsorbent–peanut husk. Desalination and Water Treatment. 233, 387-98.
39. Gul, S., Afsar, S., Gul, H., Ali, B., 2023. Removal of crystal violet dye from wastewater using low-cost biosorbent Trifolium repens stem powder. Journal of the Iranian Chemical Society. 20(11), 2781-92.
40. Mulla, B., Ioannou, K., Kotanidis, G., Ioannidis, I., Constantinides, G., Baker, M., Hinder, S., Mitterer, C., Pashalidis, I., Kostoglou, N., Rebholz, C., 2024. Removal of Crystal Violet Dye from Aqueous Solutions through Adsorption onto Activated Carbon Fabrics. C. 10(1), 19.
41. Jia, S., Song, S., Zhao, X., 2021. Selective adsorption and separation of dyes from aqueous solution by a zirconium-based porous framework material. Applied Organometallic Chemistry. 35(9), e6314.
42. Al-Kadhi, N.S., 2020. Removal of fluorescein dye from aqueous solutions using natural and chemically treated pine sawdust. International Journal of Analytical Chemistry. 2020.